Received: 24 June 2021 | Revised: 23 March 2022 | Accepted: 24 March 2022

DOI: 10.1002/humu.24375

RESEARCH ARTICLE

Human Mutation HGVS HUMAN GENOME VARIATION SOCIETY WILEY

Phenotypic and mutational spectrum of *ROR2*-related Robinow syndrome

Ariadne R. Lima[1] | Barbara M. Ferreira[2] | Chaofan Zhang[3] | Angad Jolly[3,4] | Haowei Du[3] | Janson J. White[5] | Moez Dawood[3,4,6] | Tulio C. Lins[7] | Marcela A. Chiabai[7] | Ellen van Beusekom[8] | Mara S. Cordoba[9,10] | Erica C.C. Caldas Rosa[1] | Hulya Kayserili[11] | Virginia Kimonis[12] | Erica Wu[13] | Cecilia Mellado[14] | Vineet Aggarwal[15] | Antonio Richieri-Costa[16†] | Décio Brunoni[17] | Talyta M. Canó[2,18] | Alexander A. L. Jorge[19] | Chong A. Kim[20] | Rachel Honjo[20] | Débora R. Bertola[20,21] | Raissa M. Dandalo-Girardi[22] | Yavuz Bayram[23,24] | Alper Gezdirici[25] | Elif Yilmaz-Gulec[26] | Evren Gumus[27] | Gülay C. Yilmaz[27] | Nobuhiko Okamoto[28] | Hirofumi Ohashi[29] | Zeynep Coban–Akdemir[3,30] | Tadahiro Mitani[3] | Shalini N. Jhangiani[6] | Donna M. Muzny[6] | Neysa A.P. Regattieri[9] | Robert Pogue[7] | Rinaldo W. Pereira[7] | Paulo A. Otto[21] | Richard A. Gibbs[6] | Bassam R. Ali[31] | Hans van Bokhoven[8] | Han G. Brunner[8] | V. Reid Sutton[3,32] | James R. Lupski[3,6,32,33] | Angela M. Vianna-Morgante[21] | Claudia M. B. Carvalho[3,34] | Juliana F. Mazzeu[1,2,9,35]

[1]Programa de Pós-Graduação em Ciências da Saúde, Universidade de Brasília, Brasília, DF, Brasil

[2]Programa de Pós-Graduação em Ciências Médicas, Universidade de Brasília, Brasília, DF, Brasil

[3]Department of Molecular and Human Genetics, Baylor College of Medicine, Houston, Texas, USA

[4]Medical Scientist Training Program, Baylor College of Medicine, Houston, Texas, USA

[5]Department of Pediatrics, University of Washington, Seattle, Washington, USA

[6]Human Genome Sequencing Center, Baylor College of Medicine, Houston, Texas, USA

[7]Programa de Pós-graduação em Ciências Genômicas e Biotecnologia, Universidade Católica de Brasília, Brasília, DF, Brasil

[8]Radboud University Nijmegen Medical Centre, Nijmegen, The Netherlands

[9]Faculdade de Medicina, Universidade de Brasília, Brasília, DF, Brasil

[10]Hospital Universitário de Brasília, Brasília, Brasil

[11]Medical Genetics Department, School of Medicine (KUSoM), Koç University, Istanbul, Turkey

[12]Division of Genetics and Genomic Medicine, Department of Pediatrics, University of California-Irvine, Irvine, California, USA

[13]Obstetrics and Gynecology, Stanford University, Stanford, California, USA

[14]Unidad de Genética, División de Pediatría, Pontificia Universidad Católica de Chile, Santiago, Chile

[15]Department of Orthopedics, Indira Gandhi Medical College, Snowdon, India

[16]Hospital de Reabilitação de Anomalias Craniofaciais, Bauru, Brasil

[17]Universidade Presbiteriana Mackenzie–UPM, São Paulo, Brasil

[18]Núcleo de Genética–SESDF, Brasília, DF, Brasil

Ariadne R. Lima, Barbara M. Ferreira, and Chaofan Zhang contributed equally to this study.

[†]In memoriam.

[19]Laboratório de Endocrinologia Celular e Molecular LIM25, Disciplina de Endocrinologia da Faculdade de Medicina da Universidade de São Paulo, Unidade de Endocrinologia Genética, São Paulo, Brasil

[20]Unidade de Genética, Instituto da Criança-Hospital das Clinicas HCFMUSP, Faculdade de Medicina, Universidade de São Paulo, São Paulo, Brasil

[21]Departamento de Genética e Biologia Evolutiva, Instituto de Biociências, Universidade de São Paulo, São Paulo, Brasil

[22]Programa de Mestrado Profissional em Aconselhamento Genético e Genômica Humana, Instituto de Biociências, Universidade de São Paulo, São Paulo, Brasil

[23]Department of Pathology and Laboratory Medicine, Division of Genomic Diagnostics, Children's Hospital of Philadelphia, Philadelphia, Pennsylvania, USA

[24]Perelman School of Medicine, University of Pennsylvania, Philadelphia, Pennsylvania, USA

[25]Department of Medical Genetics, Basaksehir Cam and Sakura City Hospital, Istanbul, Turkey

[26]School of Medicine, Istanbul Medeniyet University, Istanbul, Turkey

[27]Medical Genetics Department, Medicine Faculty, Mugla Sitki Kocman University, Mugla, Turkey

[28]Department of Medical Genetics, Osaka Women's and Children's Hospital, Osaka, Japan

[29]Saitama Children's Medical Center, Division of Medical Genetics, Saitama, Japan

[30]Department of Epidemiology, Human Genetics, and Environmental Sciences, Human Genetics Center, School of Public Health, UT Health, Houston, Texas, USA

[31]Department of Genetics and Genomics, College of Medicine and Health Sciences, United Arab Emirates University, Al-Ain, United Arab Emirates

[32]Texas Children's Hospital, Houston, Texas, USA

[33]Department of Pediatrics, Baylor College of Medicine, Houston, Texas, USA

[34]Pacific Northwest Research Institute, Seattle, Washington, USA

[35]Robinow Syndrome Foundation, Anoka, Minnesota, USA

Correspondence
Juliana F. Mazzeu, Faculdade de Medicina, Universidade de Brasília, DF, CEP: 70910-900, Brasil.
Email: julianamazzeu@unb.br and julianamazzeu@yahoo.com

Funding information
National Institute of Neurological Disorders and Stroke, Grant/Award Number: R35 NS105078; National Institute of General Medical Sciences, Grant/Award Number: R01 GM132589; Eunice Kennedy Shriver National Institute of Child Health and Human Development, Grant/Award Number: R03HD092569; National Human Genome Research Institute, Grant/Award Number: UM1HG006542; Fundação de Amparo à Pesquisa do Estado de São Paulo, Grant/Award Number: CEPID-2013/08028-1

Abstract

Robinow syndrome is characterized by a triad of craniofacial dysmorphisms, disproportionate-limb short stature, and genital hypoplasia. A significant degree of phenotypic variability seems to correlate with different genes/loci. Disturbances of the noncanonical WNT-pathway have been identified as the main cause of the syndrome. Biallelic variants in *ROR2* cause an autosomal recessive form of the syndrome with distinctive skeletal findings. Twenty-two patients with a clinical diagnosis of autosomal recessive Robinow syndrome were screened for variants in *ROR2* using multiple molecular approaches. We identified 25 putatively pathogenic *ROR2* variants, 16 novel, including single nucleotide variants and exonic deletions. Detailed phenotypic analyses revealed that all subjects presented with a prominent forehead, hypertelorism, short nose, abnormality of the nasal tip, brachydactyly, mesomelic limb shortening, short stature, and genital hypoplasia in male patients. A total of 19 clinical features were present in more than 75% of the subjects, thus pointing to an overall uniformity of the phenotype. Disease-causing variants in *ROR2*, contribute to a clinically recognizable autosomal recessive trait phenotype with multiple skeletal defects. A comprehensive quantitative clinical evaluation of this cohort delineated the phenotypic spectrum of *ROR2*-related Robinow syndrome. The identification of exonic deletion variant alleles further supports the contention of a loss-of-function mechanism in the etiology of the syndrome.

KEYWORDS
chromosome microarray analysis, craniofacial morphology, exonic deletion, HPO terms, next-generation sequencing, quantitative phenotyping cluster heatmap, skeletal dysplasia, WNT pathway

1 | INTRODUCTION

Robinow syndrome (RS) is characterized by a triad of craniofacial dysmorphism, disproportionate-limb short stature, and genital hypoplasia, with an extensive degree of clinical variability (Mazzeu et al., 2007; Robinow et al., 1969). More pronounced skeletal involvement and marked short stature are observed in the autosomal recessive (AR) form of RS (AR-RS), initially described as COVESDEM syndrome (COstoVErtebral Segmentation DEfects with Mesomelia; MIM# 268310) (Wadia et al., 1978). AR-RS is mostly caused by biallelic variants in the tyrosine kinase-like orphan receptor gene *ROR2* (Afzal et al., 2000; van Bokhoven et al., 2000). Autosomal recessive inheritance has also been described in a rare form of RS with biallelic variants in *NXN* (MIM# 618529) (White et al., 2018; Zhang et al., 2021). Gain-of-function (GoF) *ROR2* variants have been associated with autosomal dominant brachydactyly type B (MIM# 113000) including nonsense/frameshift variants resulting in premature termination codons (PTC) mapping to the last coding exon, or −55 bp of the penultimate exon, that escape nonsense-mediated decay (NMD) (Ben-Shachar et al., 2009; Schwabe et al., 2000).

The autosomal dominant forms of RS (AD-RS) are associated with a milder skeletal phenotype and are usually caused by heterozygous pathogenic variants in *WNT5A* (DRS1; MIM# 180700) (Person et al., 2010), *DVL1* (DRS2; MIM# 616331) (Bunn et al., 2015; White et al., 2015), *DVL3* (DRS3; MIM# 616894) (White et al., 2016), *FZD2* (White et al., 2018; Zhang et al., 2022), *or DVL2* (Zhang et al., 2022). Nevertheless, there is also one report of biallelic *WNT5A* variants in RS inherited from unaffected heterozygous parents (Birgmeier et al., 2018).

All genes associated with RS, play a role in the β-catenin-independent WNT/planar cell polarity pathway. Therefore, despite the genetic heterogeneity, the genes implicated in causing RS to date converge on the WNT signaling pathway, resulting in a recognizable clinical syndrome (White et al., 2018; Zhang et al., 2022).

The receptor tyrosine kinase-like orphan receptors (RORs) are involved in the regulation of multiple biological processes during embryonic development, including development of axial and paraxial mesoderm, nervous system, and neural crest, axial and appendicular skeleton, and kidneys. The characteristic skeletal phenotype of AR-RS includes vertebral malformations, which were observed in the *Ror2*-null mouse model and are caused by the reduced size of presomitic mesoderm (Schwabe et al., 2004). Animal model studies have also identified several WNT pathway components in the mechanisms of craniofacial and limb formation (Geetha-Loganathan et al., 2009; Nohno et al., 1999; Sisson & Topczewski, 2009).

RS-associated genes not only encode components in a common pathway, but the individual protein component directly interact with each other in signal transduction. WNT5A acts as a soluble extracellular ligand of ROR2, and together with FZD2 transmembrane receptor they trigger the DVL homologs to transduce the β-catenin independent pathway. The WNT5A-ROR2 pathway is a proposed additional branch of the noncanonical WNT-signaling network. Unlike the canonical WNT pathway, other branches of this signaling pathway are not well-defined, resulting in a paucity of information regarding constituent components (Stricker et al., 2017).

Facing the challenges in the clinical diagnosis of RS and in a first attempt to clinically differentiate the AR-RS and AD-RS forms, Mazzeu et al. (2007) investigated the frequency of clinical signs and symptoms in 88 patients with RS, considering rib fusions as indicative and potentially pathognomonic of the AR-RS form. However, despite the more severe bone involvement in AR-RS, rib fusion is not universally present in AR-RS, evident by its absence in a small proportion of molecularly-confirmed cases (Aglan et al., 2015; Mehawej et al., 2012).

The identification of the causative genes in RS further illuminated the underlying patho-mechanism of disease and enhanced the understanding of how the molecular lesions lead to the phenotypic expression. The molecular diagnosis together with quantitative deep phenotyping using Human Phenotype Ontology (HPO) terms and similarity analysis have recently become powerful tools for delineating disease contributing molecular pathways, the biology of disease, and the definition of the etiology of many syndromes, including RS (Zhang et al., 2022). A detailed phenotypic characterization of patients with an identified disease causing variant allele allows more precise genotype–phenotype correlation, delineation of allele-specific phenotypic differences, and increases the accuracy of clinical diagnosis and management.

There are few reports of AR-RS patients with a confirmed molecular diagnosis. Thirty-two different *ROR2* pathogenic variants have been identified so far in patients of different ethnicities (Table S1). Most variants were located in exons 5, 6, and 9. While truncating variant mRNAs are degraded by nonsense-mediated decay (Ben-Shachar et al., 2009), mutant protein caused by missense variants are retained in the endoplasmic reticulum and ultimately lead to the absence of the ROR2 receptor (Ali et al., 2007; Chen et al., 2005).

We report the genotype and detailed HPO-term-based quantitative phenotypic analyses of 22 patients with biallelic *ROR2* variants, aiming to further characterize and expand the phenotypic and genotypic spectrum of *ROR2* related AR-RS.

2 | SUBJECT AND METHODS

2.1 | Clinical data

Twenty-two patients with a clinical diagnosis of RS or RS-like phenotype were referred from different medical genetic clinics worldwide for identification of the causative variants and/or clarification of the definitive diagnosis for conditions with phenotypic overlap (Figures S1 and S2). Seventeen patients were referred by clinical geneticists. Five patients were evaluated by a genetic counselor specialized in the clinical phenotyping of RS, during the family conventions organized by the Robinow Syndrome Foundation (www.robinow.org). Informed consent/assent was obtained and pretest counseling was provided to all patients and/or their legal

guardians. This study was approved by the institutional ethics committee of the Faculdade de Medicina, Universidade de Brasília (CEP FM: 079/2009; 25/11/2009), and the Institutional Review Board at Baylor College of Medicine (IRB protocols no. H-43246 and no. H-29697).

The clinical information of three patients was partially included in previous publications: A16 (Beiraghi et al., 2011); A6 and A21 (Abu-Ghname et al., 2021; Conlon et al., 2021; Gerber et al., 2021; Schwartz et al., 2021; Shayota et al., 2020; Zhang et al., 2021). Patients A2, A5, A6, A8, A9, and A16 were included in the clinical review by Mazzeu et al. (2007).

Clinical data were collected using a standardized table including all clinical signs present in more than 25% of the patients with AR-RS, according to Mazzeu et al. (2007). Detailed family history, anthropometric data, radiographic images, and other investigations and results were obtained during the consultation or from patient's clinical records.

2.2 | Quantitative phenotypic analyses based on HPO terms

Phenotypes were annotated with HPO terms for each affected individual ($N = 22$). All diseases ($n = 8114$, including number symbol, plus sign, percent sign, and no symbol in OMIM) and genes ($n = 4216$, asterisk symbol in OMIM) that have been annotated with HPO terms by OMIM were downloaded from the Human Phenotype Ontology resource page (https://hpo.jax.org/app/download/annotation). Individual similarity matrices were generated with the OntologyX suite of R packages using the Lin′s semantic similarity score and the average method (Lin, 1998; Liu et al., 2019). Similarity matrices were then used to generate distance matrices of individual similarity. Hierarchical agglomerative clustering (HAC) was performed on distance matrices with the Ward's method (Ward, 1963) with the number of clusters set based on visualization of the gap statistic curve. Individual similarity scores were visualized using the ComplexHeatmap package in R, and statistical analysis of individual groups was done using the OntologyX suite. Annotation grids were generated with the OntologyX suite of packages, and then edited to exclude ancestral terms and to order columns by phenotype frequency. A cohort-to-gene and cohort-to-disease HPO analysis was performed.

These 22 individuals, 21 unrelated research subjects with RS, were separately assessed for phenotypic similarity to all (1) genes and (2) diseases with OMIM HPO annotation. HPO-annotated phenotypes for the 22 individuals were queried against all disease-associated genes ($n = 4216$) or all diseases ($n = 8114$) annotated with HPO terms by OMIM for phenotypic similarity. Lin semantic similarity scores between all pairs of the 22 individuals and all genes or diseases annotated with HPO terms were calculated. The top 10 phenotypically similar gene-associated or disease HPO term sets to each disease in the group of 31 diseases described above was parsed and duplicates removed. Every combination of two that includes one member from the group of 22 individuals and one from the top phenotypically similar gene associated phenotype matches was taken, and the p value calculated via comparison of the phenotypic similarity score between that group of two and 100,000 randomly selected groups of two from all OMIM HPO annotated genes or diseases, respectively (p value cutoff < 0.001). The gap statistic was calculated for cluster number $k = 1–11$ (gene analysis) or 8 (disease analysis), and the resultant curve was visualized to select optimal number of clusters to use. HAC analysis and visualization of phenotypic similarity and clustering was then performed as described above for RS proband phenotypes.

2.3 | Analysis of variant type-associated phenotypes

The 22 *ROR2* probands were categorized into two groups based on variant type. The missense group ($N = 7$), composed of all individuals carrying biallelic missense variants, and the loss of function (LoF) group ($N = 6$), composed of all individuals carrying biallelic LoF (nonsense and frameshifting) variants. Individuals with other variant types were not included in this analysis because of limited numbers ($N < 3$). Prevalence of each phenotype in each group was calculated. Prevalence of each phenotype across all 22 individuals and prevalence of each phenotype across all probands published in Mazzeu et al. (2007) were also included. Patient prevalence of each phenotype in each group were visualized by using the ComplexHeatmap package in R language.

2.4 | Molecular analysis

DNA was extracted from peripheral blood or saliva lymphocytes, according to standard laboratory procedures. Screening approaches for *ROR2* variants (Table 1) included targeted Sanger sequencing (patients A1, A2, A4, A6, A7, A8, A9, A16, A17, and A21), next-generation sequencing (NGS) panels (patients A3, A5, A10, A11, A14, and A19), exome sequencing (ES) (patients A12, A13, A20, and A22), multiplex ligation-dependent probe amplification (MLPA) (patients A4 and A11) and chromosome microarray (A4 and A11).

Sanger sequencing of all *ROR2* coding regions and intron-exon boundaries was performed as a first screening method for 10 patients and for confirmation of the causative variants identified through next-generation sequencing for the remaining subjects.

For four patients, screening was performed using the ION PGM™ Inherited Disease Panel, as described by the manufacturer. Library construction was carried out using the Inherited Disease Panel (IDP) and the Ion Ampliseq™ Library Kit 2.0 (Thermo Fisher Scientific), using 30 ng/primer pool of genomic DNA, following the manufacturer's recommendation. The amplicons were enriched with the Ion PGM™ Template OT2 200 Kit on the Ion OneTouch™ 2 instrument (OT2) and Ion OneTouch™ ES (Thermo Fisher Scientific). Sequencing was performed using the Ion PGM™ Sequencing 200 kit v2 on Ion Torrent PGM™ System using the Ion 318™ Chip v2 with two samples

TABLE 1 *ROR2* variants identified in 22 patients with a clinical diagnosis of the recessive form of Robinow syndrome

Patient	Disease causing variants	Protein effect	Zygosity	Novel? (Y/N)	CADD SNV PHRED	ACMG/AMP classification	Inheritance	Method
A1	c.323G>A	p.(Arg108Gln)	Hom	N	25.7	Likely Pathogenic PM2/ PP4/PP5	Parents not tested	Sanger sequencing
A2	c.323G>A	p.(Arg108Gln)	Hom	N	25.7	Likely Pathogenic PM2/ PP4/PP5	Parents not tested	Sanger sequencing
A3	c.355C>T	p.(Arg119*)	Hom	N	35.0	Pathogenic PVS1/PM2/ PP4/PP5	Parents not tested	NGS panel
A4	Seq[GRCh37]/hg19]del(9)(q22.31) chr9:g.94498192_94519323del	p.?	Hom	Y	-	Uncertain +0.45	Heterozygous parents	Sanger sequencing /MLPA/CMA
A5	c.613C>T c.1189C>T	p.(Arg205*) p.(Arg397*)	Comp Het	N, N	36.0 40.0	Pathogenic PVS1/PM2/ PP4/PP5 Pathogenic PVS1/PM2/ PP4/PP5	Parents not tested	NGS panel
A6	c.899G>T c.990delC	p.(Cys300Phe) p.(Thr331Profs*114)	Comp Het	N, N	27.4 -	Likely Pathogenic PM2/ PM3/PP3/PP4/PP5 Pathogenic PVS1/PM2/ PP4/PP5	Mother heterozygous for c.899G>T. Father not tested	Sanger sequencing
A7	c.717C>A	p.(Cys239*)	Hom	Y	37.0	Pathogenic PVS1/PM2/ PP/4PP5	Parents not tested	Sanger sequencing
A8	c.675delG	p.(Gln225Hisfs*220)	Hom	Y	-	Pathogenic PVS1/PM2/ PP4/PP5	Heterozygous parents	Sanger sequencing
A9	c.2074C>A	p.(Pro692Thr)	Hom	Y	25.7	Uncertain Significance PM2/ PP3/PP4/PP5	Heterozygous parents	Sanger sequencing
A10	c.1516_1520delinsT	p.(Ile506*)	Hom	Y	-	Pathogenic PVS1/PM2/ PP3/PP4	Heterozygous parents	NGS panel
A11	c.1970G>A Seq[GRCh37]/hg19]del(9) (q22.31) chr9:g.94371974_94844329del	p.(Arg657His) -	Comp Het	Y, Y	31.0 -	Uncertain significance PM2/ PM3/PP4 Pathogenic +1.00	Parents not tested	NGS panel/ MLPA/CMA
A12	c.494+4_494+7del	-	Hom	Y	-	Uncertain significance PM2/ PP3/PP4	Parents not tested	Exome sequencing
A13	c.2T>G	p.?	Hom	Y	20.4	Likely Pathogenic PVS1/ PM2//PP4/PP5	Heterozygous parents	Exome sequencing
A14	c.79_80delTC	p.(Ser29Profs*5)	Hom	Y	-	Pathogenic PVS1/PM2/PP4	Parents not tested	NGS panel

(Continues)

TABLE 1 (Continued)

Patient	Disease causing variants	Protein effect	Zygosity	Novel? (Y/N)	CADD SNV PHRED	ACMG/AMP classification	Inheritance	Method
A15	c.1855C>A c.2215T>C	p.(Arg619Ser) p.(Phe739Leu)	Comp Het	Y, Y	26.4 25.7	Uncertain significance PM2/PP3/PP4/PP5 Uncertain significance PM2/PP3/PP4/PP5	Parents not tested	Sanger sequencing
A16	c.1096C>T c.2207G>A	p.(Arg366Trp) p.(Arg736Gln)	Comp Het	N, Y	29.1 28.1	Likely Pathogenic PM1/PM2/PM3/PP3/PP4/PP5 Likely Pathogenic PM2/PM3/PP3/PP4/PP5	Father: c.1096C>T Mother: c.2207G>A	Sanger sequencing
A17/A18	c.623-11G>A	--	Hom	Y	-	Uncertain significance PM2/PP4/PP5/BP7	Heterozygous parents	Sanger sequencing
A19	c.2074C>A	p.(Pro692Thr)	Hom	Y	25.7	Uncertain Significance PM2/PP3/PP4/PP5	Heterozygous parents	NGS panel
A20	c.1083delG c.1324C>T	p.(His362Thrfs*83) p.(Arg442*)	Comp Het	Y, N	- 36.0	Pathogenic PVS1/PM2/PM3/PP3/PP4/PP5 Pathogenic PVS1/PM2/PM3/PP4/PP5	Father:c.1324C>T Mother:c.1083delG	Exome sequencing
A21	c.904C>T c.1970G>A	p.(Arg302Cys) p.(Arg657His)	Comp Het	N, Y	27.4 31.0	Uncertain Significance PM2/PP4 Uncertain significance PM2/PP3/PP4	Father: c.904C>T Mother: c.1970G>A	Sanger sequencing
A22	c.1100A>T c.1189C>T	p.(Asn367Ile) p.(Arg397*)	Comp Het	Y, N	26.5 40.0	Likely Pathogenic PM1/PM2/PM3/PP3/PP4/PP5 Pathogenic PVS1/PM2/PM3/PP4/PP5	Father: c.1189C>T Mother: c.1100A>T	Exome sequencing

Note: All variants are represented in NM_004560.4. CADD model GRCh37-v1.6. ACMG/AMP classification automated using Franklin (Genoox) accessed on June 15, 2021.

Abbbreviations: CADD, combined annotation dependent depletion; Comp Het, Compound Heterozygous; Hom, Homozygous; MLPA, multiplex ligation-dependent probe amplification; NGS, next-generation sequencing.

per microchip. Enrichment and sequencing were performed following the manufacturer's recommendation. The data were processed using the Ion Torrent Suite™ Server using hg19 as the reference genome for alignment, and the Ion Reporter™ Software v5.2, for variant analysis (Thermo Fisher Scientific).

Samples from four patients were submitted to ES at the Human Genome Sequencing Center (HGSC) at Baylor College of Medicine, through the Baylor-Hopkins Center for Mendelian Genomics Initiative (Posey et al., 2019). ES was performed using 0.5 µg of DNA in an Illumina (Illumina, San Diego, USA) paired-end pre-captured library constructed according to the manufacturer's protocol with modifications. Six to ten pre-captured libraries were pooled and then hybridized in solution to the HGSC in-house developed VCRome 2.1 design with custom spike-in according to the manufacturer's protocol NimbleGen SeqCap EZ Exome Library SR User's Guide with minor revisions. Illumina sequencing was performed with a sequencing yield averaging 11 Gb, samples achieved 97.5% of the targeted exome bases covered to a depth of 20× or greater with an average depth of coverage of 118.6×. In parallel to the exome workflow, a cSNP array was generated for a final quality assessment. This included orthogonal confirmation of sample identity and purity using the Error Rate In Sequencing (ERIS) pipeline developed at the HGSC. Using an "e-GenoTyping" approach, ERIS screens all sequence reads for exact matches to probe sequences defined by the variant and position of interest. A successfully sequenced sample must meet quality control metrics of ERIS SNP array concordance (>90%) and ERIS average contamination rate (<5%). Two variant discovery methods were used in parallel to prevent bias in the filtering and parsing of variants starting with the HGSC Mercury analysis pipeline (Reid et al., 2014), which moves data from the initial sequence generation on the instrument to annotated variant call files via various analysis tools including xAtlas for variant calling. In addition, we used the Genome Analysis Toolkit (GATK) HaplotypeCaller to produce joint called files with indel realignment and base recalibration in all patients that underwent ES. Candidate variants were filtered against exome data in publicly available databases, including the Genome Aggregation Database (gnomAD), the NHLBI Exome Sequencing Project (ESP) Exome Variant Server, the Atherosclerosis Risk in Communities Study (ARIC) database, and the internal Baylor-Hopkins Centers for Mendelian Genomics variant analyzer database (~13,000). In parallel, webtools were applied to parsed rare variant data that can predict functional effects of candidate variants into consideration, such as polymorphism phenotyping v2 (PolyPhen-2), sorting intolerant from tolerant (SIFT), and combined annotation dependent depletion (CADD) (Adzhubei et al., 2010; Kircher et al., 2014; Sim et al., 2012). A B-allele frequency was calculated from ES data using BafCalculator (Eldomery et al., 2017) to delineate genomic intervals showing absence of heterozygosity (AOH) as a surrogate measure for runs of homozygosity (ROH) and consistent with identity-by-descent (IBD).

Pathogenicity was ascertained automatically using Franklin (Genoox) according to ACMG/AMP guidelines (Richards et al., 2015). Variants were scored for a likelihood of damaging effect, or deleteriousness, by CADD.

Screening for deletion and duplication variant alleles affecting *ROR2* was performed by MLPA using kit P179 (MRC-Holland) in cases with no variant or when only a single variant allele was identified by Sanger sequencing or NGS. Reactions were performed according to manufacturer's protocol and analyses were performed using Coffalyser software.

Deletion in patient A11 was independently confirmed by chromosome microarray analysis, using the Cytoscan 750K platform (Thermo Scientific). The procedures for sample purification, hybridization, and washing were those described by the manufacturer and analysis was performed using CHAS software (Thermo Scientific).

Customized aCGH in 4x180K format (AMADID# 086154; Agilent Technologies), which covers RS related genes, genes related to conditions within the differential diagnosis of RS, and genes in WNT signaling pathways (837 mean probe space), was performed on genomic DNA isolated from blood obtained from subject A4 and A11. Experimental steps of aCGH, including DNA fragmentation, DNA labeling and clean-up, array hybridization, array washing, and scanning were performed as previously described (Beck et al., 2019). Junctions of deletions were then confirmed by conventional polymerase chain reaction (PCR) and Sanger dideoxy capillary sequencing. The primers used were: (1) A4 *ROR2* F: TGAAACCGTTCCCTAGGGCC; (2) A4 *ROR2* R: GGACAATCTTGTG CCCTGGA; (3) A11 *ROR2* F: CACCTCTTATGAGCCAGGCA; (4) A11 *SPTLC1* R: CGAGACCAGCCTCAGCATG.

Patients A15, A17, and A19 were screened for *ROR2* variants using NGS panels in different certified clinical laboratories. Patient 18 was screened by Sanger sequencing for the variant identified in her sister.

2.5 | Construction of *ROR2* mutants

The plasmid pcDNA3-Ror2WT-HA (Ali et al., 2007) served as a template to generate *ROR2* mutants R108Q, R366W, P693T, and R736Q. QuickChange™ Mutagenesis (Stratagene) was performed according to the manufacturer's instructions using the following primers: R108Q: Ror2-R108Q-F, GTGCAAGAGCCACGA-CAGGTCGTCATCCGGAAG and Ror2-R108Q-R, CTTCCGGATGAC-GACCTGTCGTGGCTCTTGCAC; R366W:

Ror2-R366W-F, -GGCCATGCCTACTGCTGGAACCCCGGGGGC and Ror2-R366W-R-GCCCCCGGGGTTCCAGCAGTAGGCATGGCC

CTTCCGGATGACGACCTGTCGTGGCTCTTGCAC; P693T: Ror2-P693T-F, CTTTAGCTACGGCCTGCAAACCTACTGTGGGTACTCC and Ror2-P693T-R, GGAGTACCCACAGTAGGTTTGCAGGCCGTAGCTAA AG; R736Q: Ror2-R736Q-F, GAGTTCCCAAGCCGGCAGCCCCGCTT-TAAGGAC and Ror2-R736Q-R, GTCCTTAAAGCGGGGCTGCCGGCT TGGGAACTC. The generated mutants were confirmed by Sanger sequencing.

2.6 | Cell culture, transfection, and fluorescence microscopy

The protocols used have been described previously (Ali et al., 2007). HeLa cells were cultured in Dulbecco's modified Eagle's medium (Invitrogen) supplemented with 10% fetal calf serum, 2 mM

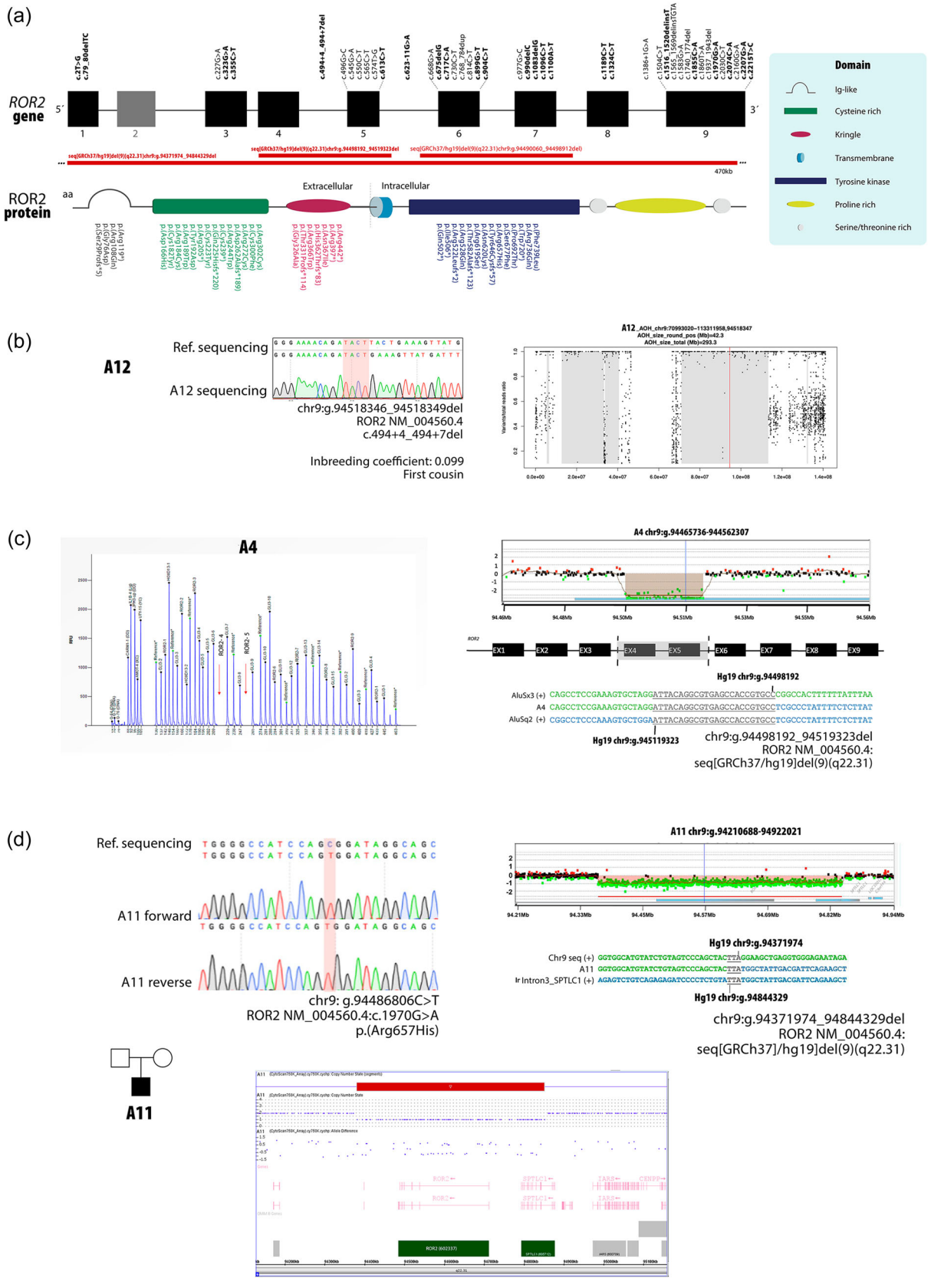

FIGURE 1 (See caption on next page)

L-glutamine, and 100 U/ml penicillin/streptomycin at 37°C with 10% CO_2. For immunofluorescence, HeLa cells were grown on coverslips in a 24-well plate for 24 h and transiently transfected using the liposomal transfection reagent FuGENE 6 (Roche Biochemicals) according to the manufacturer's instructions. In cotransfection, a mixture of 0.5 mg of EGFP-hRas, 1 mg of mRor2 wildtype or mutant DNA and 5 ml of FuGENE 6 in 94 ml of OPTIMEM I medium (Invitrogen) was applied to each well of the HeLa cells at about 60% confluence. The cells were then fixed and processed for microscopy 24 h later. For immunofluorescence, coverslip-grown HeLa cells were washed with phosphate-buffered saline (PBS), fixed in cold methanol at −20°C for 4 min, washed in PBS three times and incubated in 1X PBS containing 0.5% BSA for 15 min. The fixed cells were then incubated at room temperature for 1 h with either mouse monoclonal anti-HA antibody alone, or co-stained with both mouse monoclonal anti-HA antibody and rabbit polyclonal anti-calnexin antibody. After washing with PBS, the cells were incubated with the appropriate secondary antibodies for 1 h at room temperature, washed several times with PBS and mounted in Immuno Fluor medium (ICN Biomedicals), and visualized under a Leica DM-IRBE confocal microscope. Images were acquired using Leica TCS-NT software associated with the microscope and processed with Adobe Photoshop® (Adobe Inc.).

2.7 | Immuno-localization of *Ror2* mutant alleles

Mouse anti-HA-Tag monoclonal antibody was obtained from Cell Signaling Technology and used at 1:200 dilution for immunofluorescence, rabbit anti-calnexin polyclonal antibody from StressGen Biotechnologies and used at 1:500 dilution, Alexa Fluor 568-goat anti-mouse IgG and Alexa Fluor 488-goat anti-rabbit IgGs were from Molecular Probes and used at 1:200 dilution.

3 | RESULTS

We analyzed the genotype and phenotype of 22 patients (12 males and 10 females) from 21 unrelated families and from different ethnic backgrounds. Twelve patients have presumed consanguinity by clinical history. In four families the index cases had affected siblings (Figure S1). The only sibling pair described in detail is the pair A17/A18 for whom we had comprehensive clinical data on each affected family member.

3.1 | *ROR2* variant screening

Using different molecular approaches, biallelic causative variants were identified in all 22 patients (Table 1, Figure 1a). All families with historical report of consanguinity presented homozygous alleles. BAF calculator provided further evidence for identity-by-descent and thus confirmed the consanguinity in the two homozygous cases where such data were available (A12 and A13) (Figure 1b). In total, 25 different putatively pathogenic variants were found in 21 patients: including 10 missense, 5 nonsense, 5 small indels, and 2 large deletions. Two patients had a splicing variant, and one patient had a variant affecting the initiation codon. Sixteen of them (64%) are novel variants not yet reported in RS.

In patient A4, exons 4 and 5 of *ROR2* could not be amplified by PCR, which suggest an exonic deletion. MLPA was then performed and confirmed that these two exons were deleted in both alleles (c.(431_494 + 60)_(574_672)del). Customized array CGH followed by Sanger sequencing mapped the breakpoints within introns 3 and 5 Seq [GRCh37]del(9)(q22.31) NC_000009.11:g.94498192_94519323del) (Figure 1c).

In patient A11 (Figure 1d), a single variant (c.1970G>A, p.Arg657His), was called as homozygous by NGS analysis software. Since there was no reported history of consanguinity, and only one allele was detected for other SNPs in *ROR2*, copy-number investigation by MLPA and chromosome microarray were performed, and a 470 kb deletion encompassing the *ROR2* and *SPTLC1* genes was identified–arr[hg19] 9q22.31(94,381,136-94,851,388)x1. Customized array CGH followed by Sanger sequencing confirmed the proximal breakpoint upstream of *ROR2* and the distal breakpoint at intron 3 of *SPTLC1* (Seq[GRCh37] del(9)(q22.31) NC_000009.11:g.94371974_94844329del).

In eight unrelated patients, compound heterozygous variants were identified. In four families (A16, A20, A21, and A22) Sanger sequencing of both parents confirmed that the variants were *in trans*. For A6, TA cloning of exons 6 and 7 amplified as a single PCR product confirmed that the two variants were present in trans. Patient A11 had compound heterozygosity for a large deletion and a missense variant. Parental samples of the patients A5 and A15 were not available (Table 1).

FIGURE 1 *ROR2* variants causative of AR-RS. (a) Localization of variants described in the present study and in previous reports in relation to their position in the exons and protein domains. Novel variants are highlighted in bold. (b) Sanger sequencing chromatogram for patient A12 carrying a homozygous variant in *ROR2*. AOH plot shows that this variant is within an AOH region of 42.3 Mb. (c) Electropherogram of P179 MLPA reaction showing a homozygous deletion of probes corresponding to exons 4 and 5 of *ROR2*. Customized array CGH plots confirms the 21 kb deletion. Breakpoints determined by Sanger sequencing are represented below. (d) Sanger sequencing chromatogram for patient A11 carrying a hemizygous variant in *ROR2*. Chromosome microarray analysis showing a 470 kb deletion including whole *ROR2* and partial *SPTLC1* genes. Breakpoints determined by Sanger sequencing are represented below. AOH, absence of heterozygosity; AR-RS, autosomal recessive form of Robinow syndrome; MLPA, multiplex ligation-dependent probe amplification

TABLE 2 Clinical signs and symptoms in patients with biallelic *ROR2* variants grouped according to their frequency

Frequency %	Clinical signs
75–100	Prominent forehead (100%) Hypertelorism (100%) Wide nasal bridge (95.45%) Short nose (100%) Abnormality of the nasal tip (100%) Anteverted nares (95.45%) Midface retrusion (95.45%) Downturned corners of mouth (77.27%) Gengival overgrowth (77.27%) Bifid tongue (77.27%) Abnormalities of the dentition (75%) Short stature (100%) Mesomelia (100%) Short palms (86.36%) Clinodactyly (80,95%) Brachydactyly (100%) Rib fusion (86.36%) Hemivertebrae (86.36%) Micropenis (100%)
50–74	Proptosis (63.63%) Long eyelashes (72.72%) Long palpebral fissures (68.18%) Upslanted palpebral fissures (50%) Depressed nasal bridge (68.18%) Long philtrum (50.00%) Triangular mouth (72.72%) Thin upper lip vermilion (59.09%) Micrognathia (68.18%) Retrognathia (68.18%) Low-set ears (66.66%) Short neck (63.63%) Scoliosis (68.18%) Limited pronation/supination of forearm (65%) Broad thumbs (59.09%) Cryptorchidism (50.00%)
25–49	Dowslanted palpebral fissures (31.81%) Epicanthus (31.81%) Short philtrum (27.27%) Hypoplasia of the tongue (35.29%) Highly narrow palate (41%, 17%) Tooth agenesis (30.00%) Pectus excavatum (47.61%) Nail dysplasia (38.09%) Syndactyly (28.57%) Single transversal palmar crease (26.31%) Broad halux (47.05%) Hypoplastic labia minora (36.36%)
5–24	Melanocytic nevus (20.00%) Ptosis (13%, 63%) Strabismus (19.04%) Oral cleft (22.72%) Microtia (9%, 52%) Camptodactyly (19.04%) Hip dislocation (15.78%) Hypospadias (20.00%) Hypoplastic labia majora (16.67%) Sacral dimple (5%, 26%) Inguinal hernia (15.78%) Abnormal heart morphology (18.18%) Abnormality of the kidney (14.28%) Hearing impairment (13.63%)

3.2 | Characterization of DNA rearrangement alleles at the *ROR2* locus

Detailed characterization of the large deletions allowed precise identification of the breakpoints. In patient A11, the proximal breakpoint maps to an intergenic region upstream of *ROR2* and distal breakpoint maps to *SPTLC1* intron 3. A TTA microhomology at the breakpoint junction (Figure 1d) suggests that the deletion arose by microhomology-mediated break induced replication or by non-homologous end-joining (Carvalho & Lupski, 2016).

Patient A4 has an exonic deletion of exons 4 and 5 of *ROR2*. Breakpoint mapping confirmed the breakpoints as intronic, revealing a 21 kb genomic deletion, thus confirming deletion of both exons. A 24 bp region within *Alu* elements was identical in both introns (Figure 1c), suggesting that this deletion was mediated by AAMR (*Alu*-*Alu* mediated rearrangement). This rearrangement is similar to *Alu*-mediated CNVs reported at other disease loci, due to breakpoint microhomology, small size, and rearrangement between different *Alu* family members (Song et al., 2018). The genomic instability score for *ROR2* as calculated from AluAluCNVpredictor, (http://alualucnvpredictor.research.bcm.edu:3838/), 0.506 for RefSeq genes, suggests the possibility for encountering other exonic deletion alleles at this locus.

3.3 | Immuno-localization of *Ror2* mutant alleles

We generated mutant *Ror2* alleles for four different missense variants identified in our cohort (R108Q, and R366W, located at the extracellular part of Ror2 receptor and P692T and R736Q located at the intracellular part of Ror2 receptor). Co-expression of Ror2 and EGFP-hRas or calnexin in Hela-cells showed that wild-type Ror2 localizes predominantly to the plasma membrane, while mutant Ror2 proteins do not migrate to the plasma membrane and are retained to the endoplasmic reticulum (Figures S3 and S4). The results did not differ for mutations localized at the intracellular or extracellular domains (data not shown).

3.4 | Phenotype analysis

Phenotypes of the 22 patients with biallelic variants in *ROR2* are summarized in Table 2 (Detailed phenotype described in Table S2) and the photographs from available patients are shown in Figure 2. All

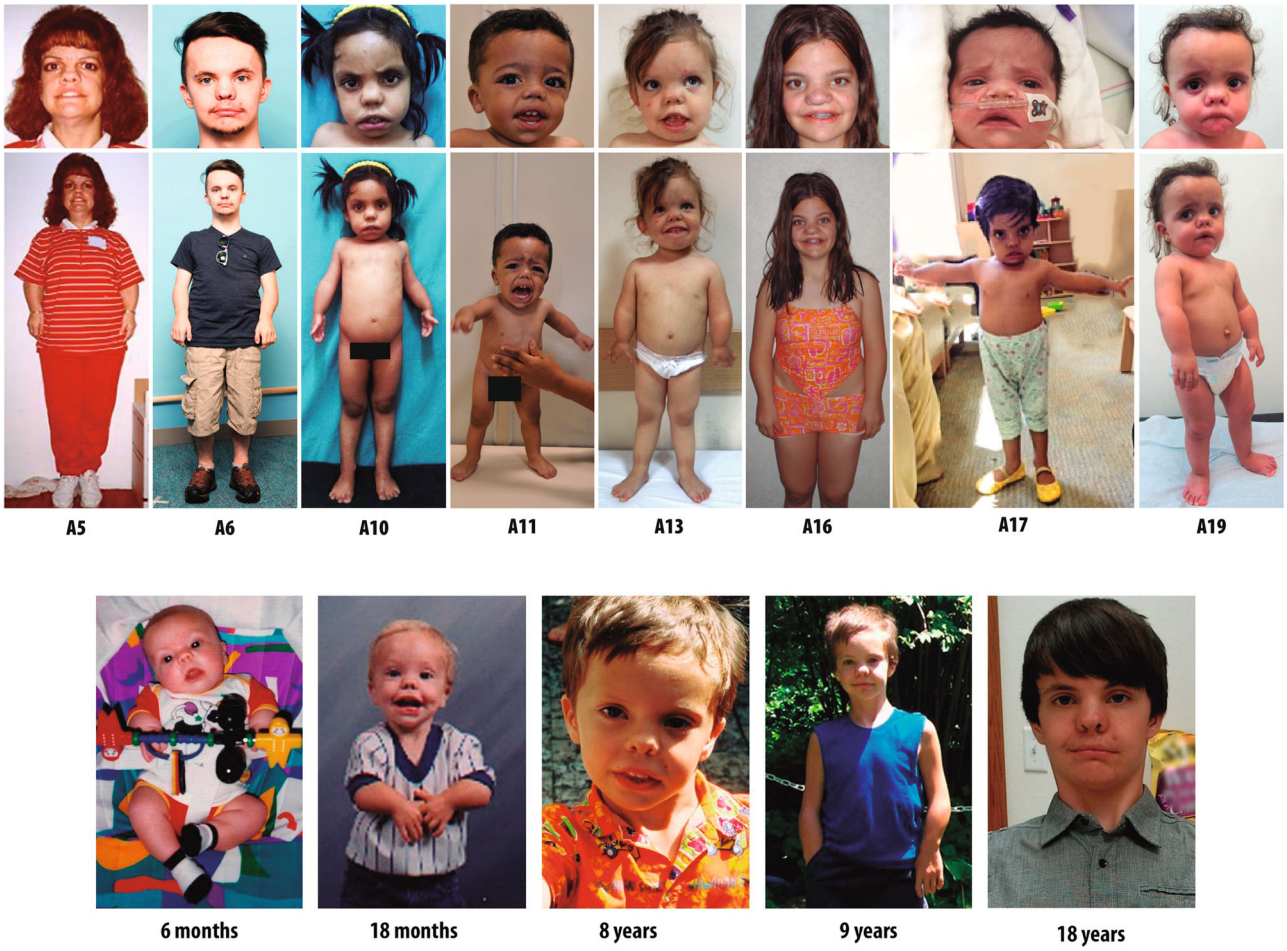

FIGURE 2 Facial and whole-body photographs of eight individuals from our cohort showing the spectrum of *ROR2*-related Robinow syndrome. All individuals exhibit typical dysmorphic features that characterize the syndrome. Patient A6 is shown at different ages to document the evolving facial gestalt

patients manifested at least 16/61 clinical features; 11 clinical features were present in more than 90% of the cohort, and 19 features, in more than 75%, pointing to an overall consistent phenotype.

Phenotypic features were classified into four groups, according to frequency: more than 75%, between 50% and 75%, between 25% and 50%, and below 25%. Prominent forehead, hypertelorism, short nose, abnormality of the nasal tip, brachydactyly, mesomelic limb shortening, short stature, and micropenis were present in all patients. Midface retrusion, wide nasal bridge, anteverted nares, downslanted mouth corners, bifid tongue, gum hyperplasia, abnormalities of the dentition, short palms, clinodactyly, hemivertebrae, and rib fusion were present in more than 75% of subjects. Therefore, these features should be considered as major defining phenotypic criteria in the clinical diagnosis of *ROR2*-related Robinow syndrome. Three patients did not present rib fusions, a sign formerly considered pathognomonic for AR-RS (Mazzeu et al., 2007). Intraoral manifestations were also prevalent (above 75%), including bifid tongue, gingival overgrowth, and abnormalities of the dentition. Genital hypoplasia was present in all male patients, but in less than 50% of the females. Major congenital anomalies, such as abnormal heart and kidneys were present in less than 25% of the patients. Hypoplasia of the tongue was present in 35% of the patients and considered a novel phenotypic feature, not previously associated with AR-RS.

3.5 | Quantitative assessment of RS clinical phenotypes

To quantify and visualize genotype–phenotype correlations, semantic similarity scores were calculated using an HPO-based analysis. Phenotypic similarity scores between each AR-RS proband and OMIM annotated gene phenotypes were calculated and visualized in a cluster heatmap.

Subjects with *ROR2* variants in our cohort were clustered with *DVL1*, *WNT5A*, *ROR2*, *DVL3*, and *NXN* gene phenotypes (Figure 3). Three different subclusters were observed: one cluster included patients A1, A2, and A21, all carrying missense variants only. The second subcluster included patients with at least one LoF allele (A3, A13, A6, A8, A14, A11, A20) and a third cluster was composed of two siblings (A17 and A18), who both carry biallelic splicing variants. No

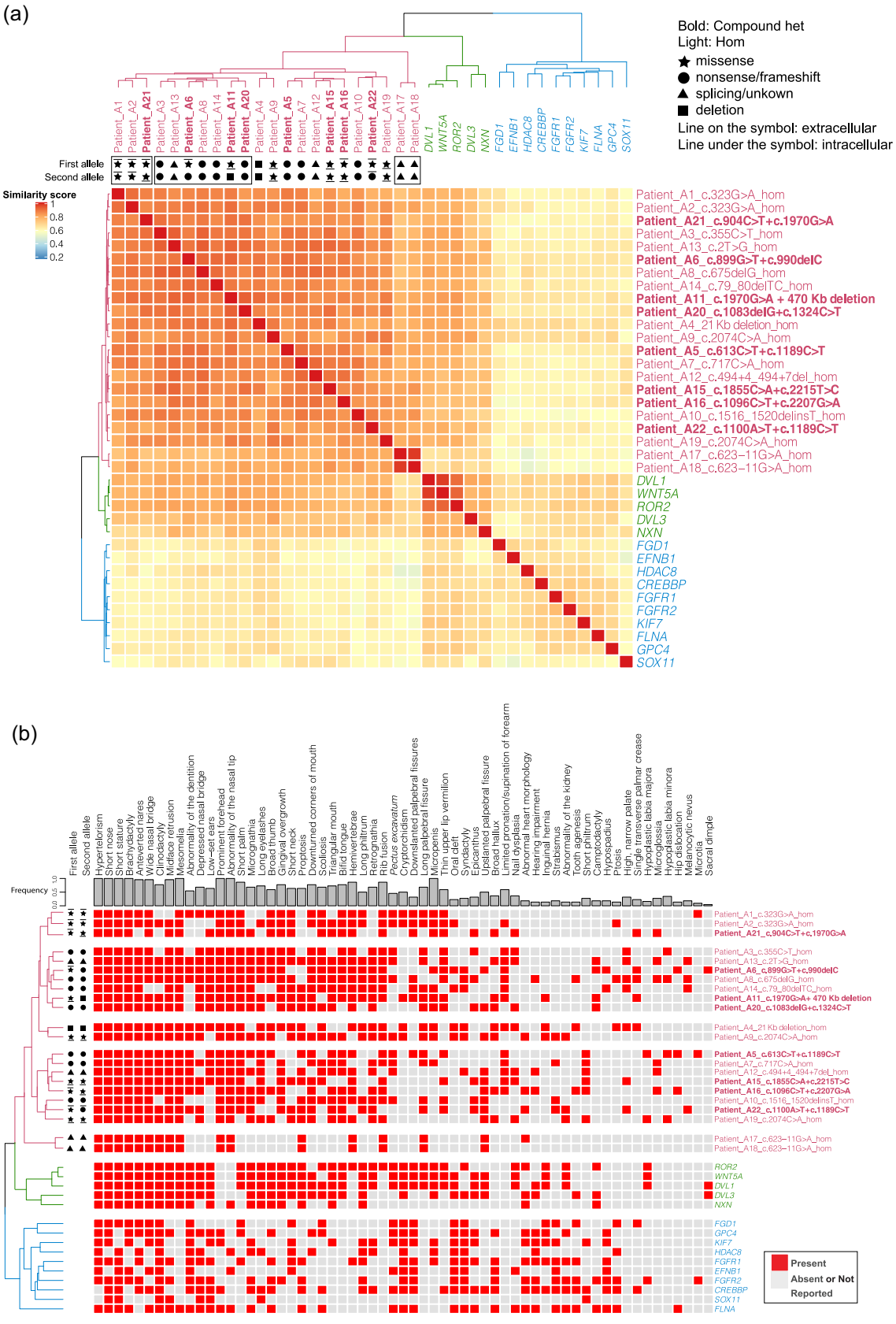

FIGURE 3 (See caption on next page)

difference was observed between patients with compound heterozygous variants and patients with homozygous variants. Variants affecting extracellular or intracellular domains did not cluster as shown in Figure 3, suggesting that domain localization does not contribute to clinical phenotypic variability in this cohort.

To investigate whether there are mutation-type specific phenotypes as suggested by the initial heatmap analysis, we sorted the cohort for biallelic missense variants ($N = 7$) and biallelic LoF variants ($N = 7$) (Figures 5 and S5). Such analysis revealed that none of the patients in the missense group had camptodactyly, hypospadia, or melanocytic nevus and long palpebral fissures, whereas low-set ears, micrognathia, and retrognathia were less-frequent in this group. In contrast, patients with biallelic LoF variants do not present cryptorchidism, abnormal heart morphology, inguinal hernia, and abnormality of the kidney whereas a few patients ($N = 3/7$) had a broad thumb.

The overall clinical phenotype was consistent in all patients as the majority of clinical signs were present in all patients independently of the type of variant (Figure 5). However, some signs were more prevalent (difference value > 28%) in the missense or LoF groups allowing discrimination between them (Figure 5).

Cryptorchidism, broad hallux, broad thumbs, abnormal heart morphology, abnormalities of the kidney, short neck, and upslanted palpebral fissures were more prevalent in patients with biallelic missense variants. Low-set ears, retrognathia, long palpebral fissures, hypoplastic labia minora, pectus excavatum, limited pronation/supination of forearm, hypospadia, melanocytic nevus, highly narrow palate, micrognathia, and epicanthus were more prevalent in the LoF group.

A similarity analysis between *ROR2* subjects and OMIM annotated disease phenotypes showed that *ROR2* subjects strongly clustered with other forms of RS caused by variants in *WNT5A*, *DVL1*, *DVL3*, and *NXN*. FZD2_OMOD2 grouped into a distinct cluster. Diseases that have phenotypic overlap with RS are matched using a less stringent p value cutoff ($p = 0.005$). This aided in viewing the similar sets of diseases to *ROR2* patient phenotypes, however, subclusters were more poorly resolved due to the increased number of phenotype sets to cluster.

4 | DISCUSSION

Here we report a cohort of 22 individuals with AR-RS caused by biallelic *ROR2* variants. Twenty-five disease-causing variants in *ROR2* were identified, and 16 of these were novel. Although most of the variants were missense, further description of frameshift, initiation site, splice-site variants, and large exonic deletion adds to the evidence that the syndrome is caused by biallelic loss-of-function variants and to the mutational and allelic complexity for this rare disease trait.

Six of the detected variants have been previously described (Table S1). The majority of the previous reports of AR-RS were from Turkey potentially due to the high frequency of consanguineous marriages. However, 13 different variants have been described in Turkish patients, which is inconsistent with a founder effect and more suggestive of the Clan Genomics hypothesis proposing recently arisen biallelic rare alleles are more likely to be unmasked due to identity-by-descent homozygosity (Lupski, 2021; Lupski et al., 2011).

The *ROR2* gene comprises nine exons. Disease-causing variants were more frequent in exons 5, 6, and 9, usually affecting the extracellular domains, though variants affecting the tyrosine kinase domain were also identified (Figure 1A, Table 1). None of the variants modified interdomain regions which is consistent with previous studies showing that variants affecting interdomain regions can act as gain-of-function (GoF) alleles and cause brachydactyly Type B (Schwabe et al., 2000). Considering all single-nucleotide variants in *ROR2* described in patients with AR-RS (Table S1) most of them (22/36) occurred at CpG nucleotides. Cytosine residues in CpG dinucleotides might undergo modifications such as methylation, deamination, and halogenation that can contribute to the formation of mutational hotspots (Sassa et al., 2016). The preponderance of alleles involving CpG is also consistent with Clan Genomics and the derivation of the allele as a new mutation in antecedent generations of the clan that is then brought to homozygosity by IBD (Lupski, 2021; Lupski et al., 2011).

Patient A11 had a possible homozygous variant detected by NGS however the parents were not consanguineous. Further studies showed a large deletion of the other allele encompassing the entire *ROR2* and part of *SPTLC1* genes. Interestingly, heterozygous *SPTLC1* variant alleles are associated with Hereditary Sensory and Autonomic Neuropathy Type 1A

FIGURE 3 Semantic similarity heatmap and phenotypic annotation grid results between research subjects with biallelic *ROR2* variants and significantly similar OMIM annotated known disease gene phenotypes. (a) *Hierarchical agglomerative clustering (HAC) and visualization of quantitative phenotypic similarity. The dendrogram shown at the top and to the left of the heatmap is based on HAC analysis of the dissimilarity matrix produced from Lin semantic similarity scores and with k set to 3. Unique clusters are represented by different colors, individual probands, and significantly similar known disease genes are labeled on top of and to the right of the heatmap. Within the heatmap, dark red indicates a higher similarity while dark blue indicates lower similarity. A key is provided on the left. Bold: subjects who have compound heterozygous variant alleles. Light font type: subjects who have homozygous variant alleles. Star: missense variants. Circle: loss of function (LoF) variants including nonsense variants and frameshifting variant alleles. Triangle: splicing variants or variants with unknown consequence. Rectangle: large exonic deletion (> 50 bp) variant alleles. Line on the symbol: variants in the extracellular region. Line under the symbol (i.e., underlined font): variants in the intracellular region. (b) Phenotypic annotation grid. Phenotypic annotation grid of phenotypes of all subjects and significantly similar known disease genes. To interpret and understand biology of phenotypes driving semantic similarity in these analyses, human phenotype ontology (HPO) terms associated with all subjects and significantly similar known disease genes were annotated and visualized in a gridded array format. Red indicates presence of a phenotype while gray represents absence or not reported. Probands and significantly similar known disease genes are labeled to the right (italicized gene symbols) and are ordered by HAC. The frequency of each phenotype in probands from this cohort is shown on top of the grid

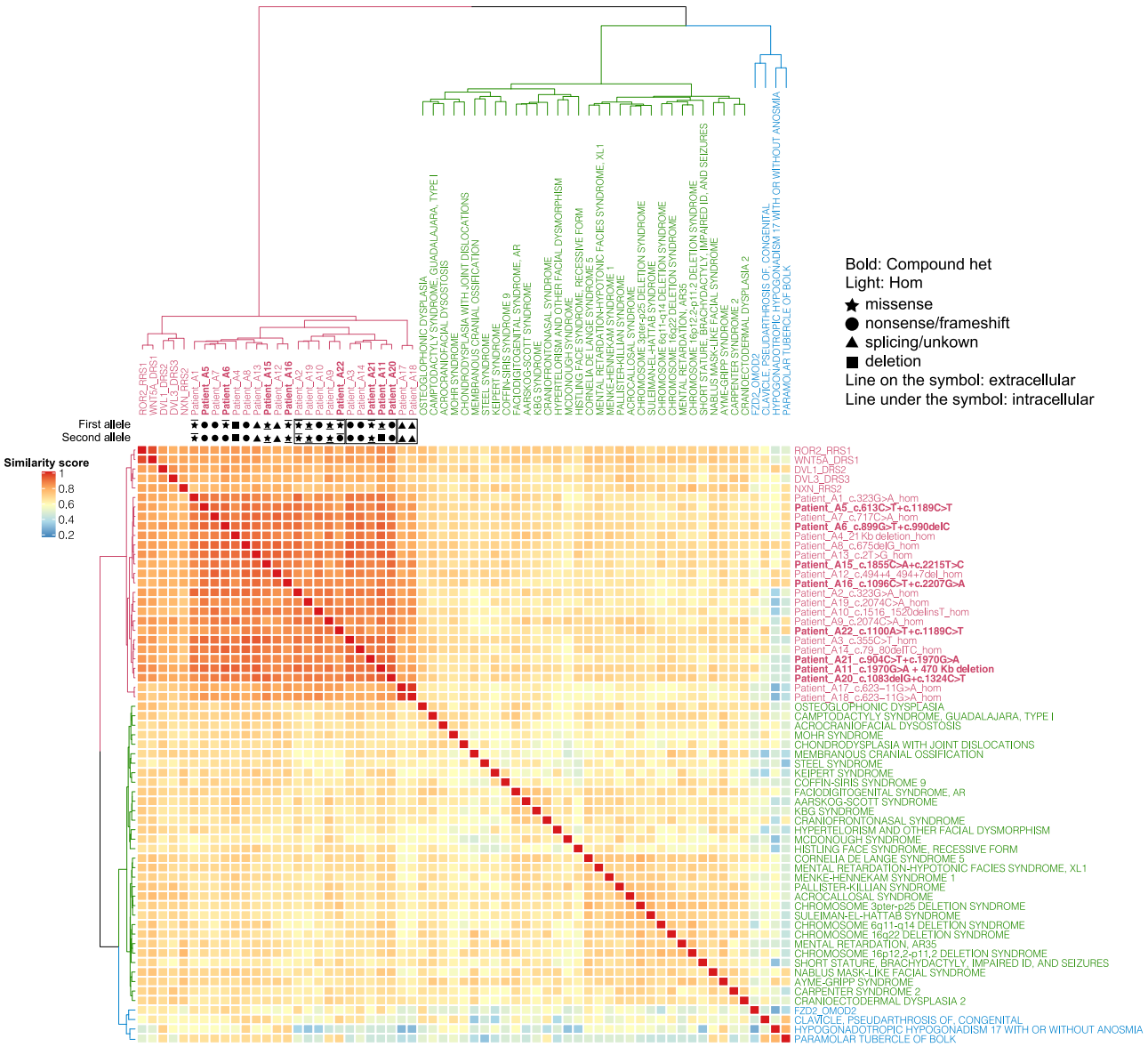

FIGURE 4 Semantic similarity heatmap between *ROR2* subjects and significantly similar OMIM annotated known disease phenotypes ($p < 0.005$). The dendrogram shown at the top and to the left of the heatmap is based on HAC analysis of the dissimilarity matrix produced from Lin semantic similarity scores and with k set to 3. Unique clusters are represented by different colors, individual probands, and significantly similar known diseases are labeled on top of and to the right of the heatmap. Within the heatmap, dark red indicates a higher similarity while dark blue indicates lower similarity. A key is provided on the left. Bold: subjects who have compound heterozygous variant alleles. Light font type: subjects who have homozygous variant alleles. Star: missense variants. Circle: LoF variants including nonsense variants and frameshifting variant alleles. Triangle: splicing variants or variants with unknown consequences. Rectangle: large exonic deletion (>50 bp) variant alleles. Line on the symbol: variants in the extracellular region. Line under the symbol (i.e., underlined font): variants in the intracellular region

(HSANIA; MIM# 162400). Whether this specific *SPTLC1* exonic deletion allele behaves as a LoF or GoF mutation remains to be explored.

According to ACMG/AMP (Richards et al., 2015), 11 variants were classified as pathogenic, six as likely pathogenic and 10 as uncertain significance. The variants classified as uncertain failed PM1 criteria for being out of mutational hotspots. In our cohort, disease-causing variants were identified throughout the gene except for exons 2 and 4, the smaller *ROR2* exons. Therefore, we did not find evidence of mutational hotspots in *ROR2* and so it seems that this PM1 classification criteria is not useful for *ROR2* variant classification.

Phenotypic analysis comparing missense variant alleles to LoF variants showed minor differences as depicted in Figure 5. These results are discordant with functional studies that demonstrate retention of ROR2 mutant proteins to the endoplasmic reticulum (Figures S3 and S4; Ali et al., 2007) as well as loss-of-function alleles from absent mRNA due to degradation by NMD surveillance mechanism. (Ben-Shachar et al., 2009). This partial genotype–phenotype correlation might indicate a residual function of *ROR2* in patients with missense variants.

Patients carrying variants that affect the extracellular or intracellular ROR2 domains do not cluster according to this feature

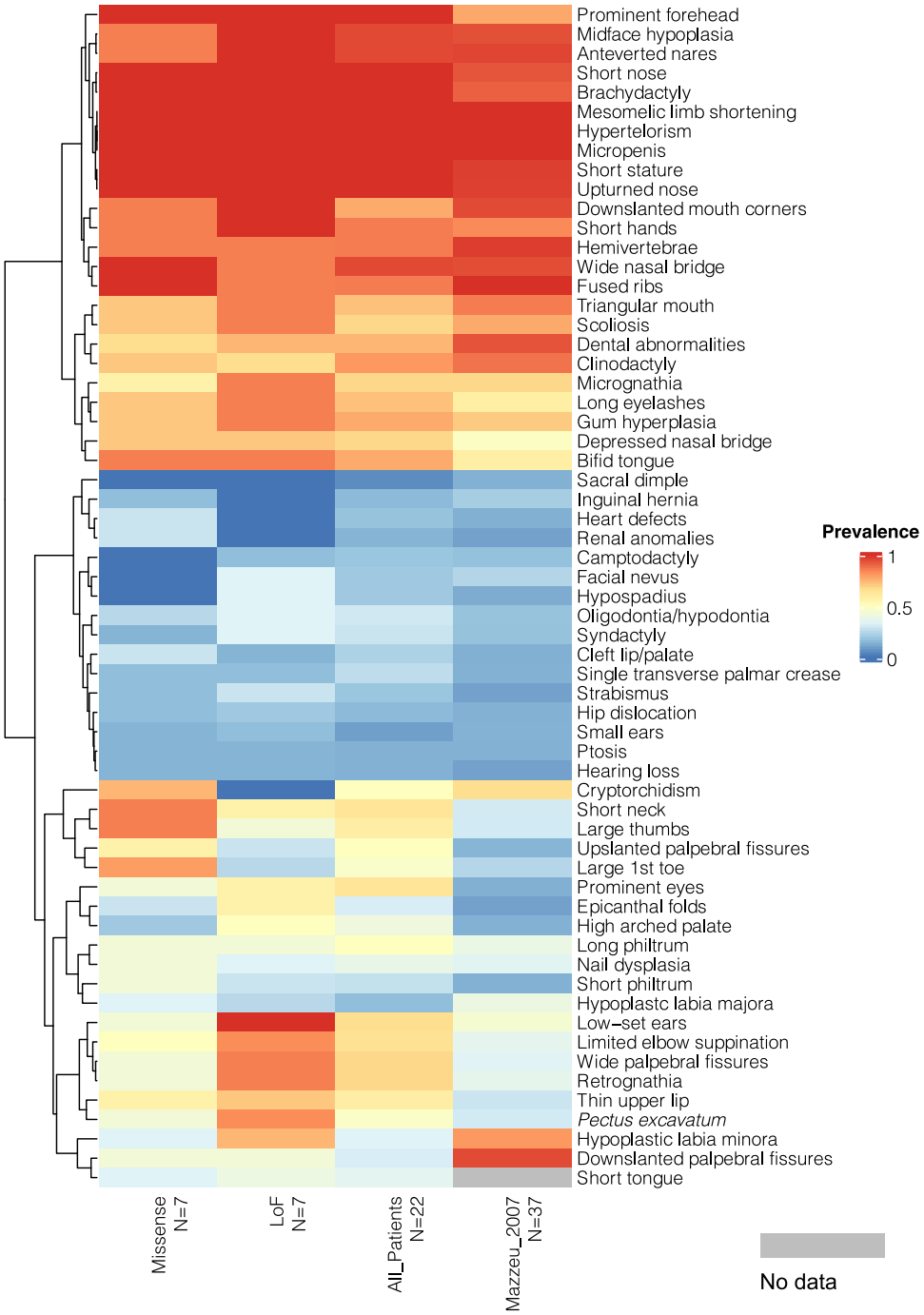

FIGURE 5 Phenotypic analysis of subjects with biallelic missense variants and LoF variants. Prevalence (0–1.0) of phenotypes in subjects with biallelic missense variants (A1, A2, A9, A15, A16, A19, A21), biallelic LoF variants (A3, A5, A7, A10, A14, A20), all subjects ($N = 22$), and subjects published in Mazzeu et al., 2007 ($N = 37$) is displayed by heatmap. Probands with other mutation types were not included in this analysis because of their limited numbers ($N < 3$). Within the heatmap, red indicates a higher prevalence while blue indicates lower prevalence; light gray indicates these specific data are not available. The phenotypes are ordered by dendrogram shown on the left based on hierarchical agglomerative clustering (HAC) analysis. A prevalence key is provided on the right

as shown in Figure 3, indicating that location of the variant in the protein may not be relevant for the overall clinical phenotype. This is consistent with the retention of all missense variants affecting intracellular or extracellular domains in the endoplasmic reticulum (Figures S3 and S4; Ali et al., 2007).

We also showed that subjects with *ROR2* variants clustered with phenotypes associated with other non-*ROR2* gene forms of the syndrome confirming the identity of Robinow syndrome as a single syndrome with genetic heterogeneity and confirming that disruption of this pathway leads to a specific group of phenotypes (Figure 4).

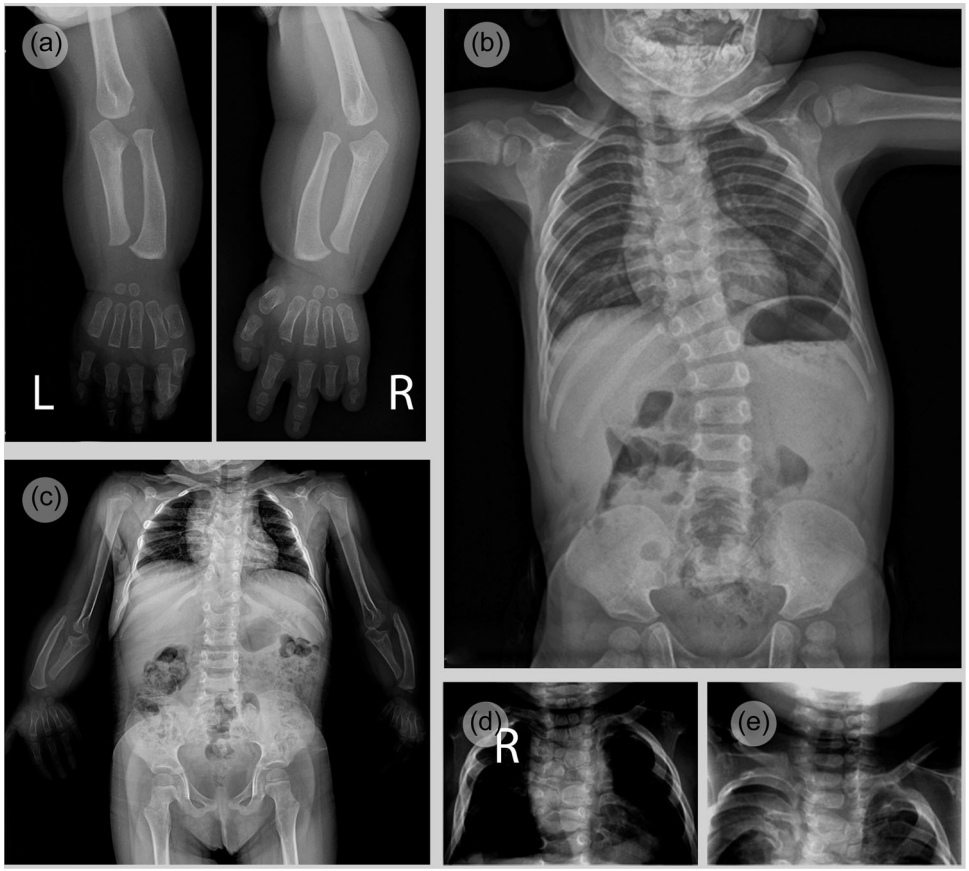

FIGURE 6 Radiographic images illustrative of major skeletal defects in AR-RS. (a) Upper limb showing mesomelia, brachydactyly with pronounced shortening of distal phalanges and absence of medial and distal phalanges of fourth finger. (b) Thoracic scoliosis due to multiple hemivertebra (c) Multiple hemivertebra, butterfly vertebrae, rib fusions, and mesomelia with malformation of the olecranon and coronoid process. Absence of the humero-radial joint. (d, e) Hemivertebra

This is in accordance with our recent phenotypic analysis of dominant RS showing that *ROR2*-RS was closely clustered with other gene forms of the syndrome (Zhang et al., 2022).

The overall phenotype of the patients reported herein is in accordance with the previous clinical characterization of AR-RS. Though some discrepancies were observed in relation to the report of Mazzeu et al. (2007), most clinical signs had similar frequencies in both studies (Tables 2 and S2, Figure 5). Minor discrepancies appeared more evident in clinical signs with mild clinical impact that might have been unreported or overlooked but could still be present. Clinical signs present in all patients (prominent forehead, hypertelorism, short nose, abnormality of the nasal tip, brachydactyly, mesomelic limb shortening, short stature, and micropenis), as well as those present in more than 75% of subjects (midface retrusion, wide nasal bridge, anteverted nares, downslanted mouth corners, bifid tongue, abnormalities of the dentition, short palms, clinodactyly, hemivertebrae, and rib fusion), should be considered when evaluating variants of uncertain significance in *ROR2*.

All skeletal changes (short stature, brachydactyly, clinodactyly, mesomelia, rib fusion, and hemivertebrae) had frequencies above 75%. Craniofacial characteristics were also consistent between different patients, including a prominent forehead, hypertelorism, midface retrusion, wide nasal bridge, short nose, abnormality of the nasal tip, anteverted nares, and downturned corners of mouth likely providing the recognizable pattern allowing clinical diagnosis (Table 2).

As with many craniofacial disorders, facial characteristics become attenuated with age in RS patients. We have followed up five patients through adulthood. The typical facial characteristics are very prominent in early childhood, but become less pronounced in adulthood (Figure 2b). An important consideration in the diagnosis of AR-RS is the characterization of the skeletal defects, considering their high prevalence. Therefore, thorough radiological documentation is essential for clinical diagnosis and management. As a diagnostic tool, the most important findings are mesomelia, brachydactyly, rib fusions, and hemivertebrae, as depicted in Figure 6. The variable severity of the vertebral defects is remarkable, some patients having a single hemivertebrae while others have all vertebrae involved with a major impact on prognosis (Figure 6). The presence of rib fusions is highly suggestive of AR-RS diagnosis. Despite the previous report of two patients with AR-RS without rib fusions (Aglan et al., 2015; Mehawej et al., 2012), also absent in Patients A12, A20, and A22, other diagnoses should also be considered, including other forms of the syndrome. Scoliosis is also a common finding that

progresses with age and is the result of multiple vertebral anomalies. In our cohort it has been described in 69% of the patients. Patients without scoliosis were usually evaluated at a very young age except for patient A5, an adult woman.

Brachydactyly was also described in all patients, although it might consist of a minimal shortening of distal phalanges or even absence of distal and medial phalanges, as shown in Figure 6. Clinodactyly is also frequent (81.8%) and some patients might also present syndactyly (28.6%).

Individuals of all ages had short stature and the final height of five adults, both females, and males, ranged between 128 and 145 cm (<3rd centile) in our cohort.

Genital anomalies do not have a major impact on female patients but are a major concern for males. At birth, the penis can be extremely small and buried, often accompanied by cryptorchidism (50%), requiring chromosomal confirmation of the genetic sex (Gerber et al., 2021). Psychological follow-up is recommended. The few male adults followed have reported normal erection and significant growth of the penis after puberty.

This study provides an in-depth quantitative clinical delineation of the *ROR2*-related recessive Robinow syndrome in a large cohort of patients from diverse ethnic background originating from multiple continents and with confirmed molecular diagnoses. Sixteen novel variants were detected that mapped throughout the coding regions of *ROR2*, with no evident hot-spots. Both a total gene deletion allele and an exonic deletion CNV allele were characterized; the latter formed by AAMR. Despite consistency of the overall phenotype, minor phenotypic differences were observed in missense and LoF cases. Functional data and the identification of large deletions further supports the LoF mechanism in the etiology of the *ROR2*-related Robinow syndrome.

ACKNOWLEDGMENTS

We thank all the patients and their families, specially the Robinow Syndrome Foundation, for participating in the study. This study was partially supported by Fundação de Amparo à Pesquisa do Estado de São Paulo (FAPESP-CEPID 2013/08028-1), Conselho Nacional de Desenvolvimento Científico e Tecnológico (CNPq), Coordenação de Aperfeiçoamento de Pessoal de Ensino Superior (CAPES), United States National Human Genome Research Institute (NHGRI)/National Heart Lung and Blood Institute (NHLBI) grant number UM1HG006542 to the Baylor-Hopkins Center for Mendelian Genomics (BHCMG), the National Institute of Neurological Disorders and Stroke (NINDS) R35 NS105078 (James R. Lupski), the National Institute of General Medical Sciences (NIGMS): R01 GM132589 (Claudia M. B. Carvalho), the Eunice Kennedy Shriver National Institute of Child Health & Human Development (NICHD) R03HD092569 (Claudia M. B. Carvalho and V. Reid Sutton).

CONFLICTS OF INTEREST

Baylor College of Medicine (BCM) and Miraca Holdings have formed a joint venture with shared ownership and governance of the Baylor Genetics (BG), which performs clinical microarray analysis and clinical exome sequencing and whole genome sequencing. J. R. L. serves on the Scientific Advisory Board of the BG. J. R. L. has stock ownership in 23andMe, is a paid consultant for Regeneron Genetics Center, and is a coinventor on multiple United States and European patents related to molecular diagnostics for inherited neuropathies, eye diseases, genomic disorders and bacterial genomic fingerprinting. The Department of Molecular and Human Genetics at Baylor College of Medicine derives revenue from molecular genetics and clinical genomics testing offered at BG. The other authors declare no competing financial interests.

DATA AVAILABILITY STATEMENT

The accession numbers for identified variants were deposited in ClinVar (http://www. https://www.ncbi.nlm.nih.gov/clinvar/) with the following identifiers: SCV001441486–SCV001441509. The dbGAP accession number for exome sequences, for which informed consent for data sharing in controlled-access databases has been provided, is dbGAP:phs000711.v5.p1 (https://www.ncbi.nlm.nih.gov/gap/).

ETHICS STATEMENT

Patients or their legal guardians signed an informed consent declaration, including consent for publication and the study was approved by the institutional ethics committee of the Faculdade de Medicina, Universidade de Brasília (CEP FM: 079/2009; 25/11/2009) and the Institutional Review Board at Baylor College of Medicine (IRB protocols no. H-43246 and no. H-29697). Informed consent was obtained from all patients for the use of photos.

WEB RESOURCES

http://www.omim.org
http://www.robinow.org
http://www.genoox.com
https://cadd.gs.washington.edu

ORCID

Haowei Du http://orcid.org/0000-0001-9052-1587
Nobuhiko Okamoto http://orcid.org/0000-0001-5415-656X
Robert Pogue http://orcid.org/0000-0002-8789-3512
James R. Lupski http://orcid.org/0000-0001-9907-9246
Juliana F. Mazzeu http://orcid.org/0000-0002-6161-0510

REFERENCES

Abu-Ghname, A., Trost, J., Davis, M. J., Sutton, V. R., Zhang, C., Guillen, D. E., Carvalho, C., & Maricevich, R. S. (2021). Extremity anomalies associated with Robinow syndrome. *American Journal of Medical Genetics, Part A*, *185*(12), 3584–3592. https://doi.org/10.1002/ajmg.a.61884

Adzhubei, I. A., Schmidt, S., Peshkin, L., Ramensky, V. E., Gerasimova, A., Bork, P., Kondrashov, A. S., & Sunyaev, S. R. (2010). A method and server for predicting damaging missense mutations. *Nature Methods*, *7*(4), 248–249. https://doi.org/10.1038/nmeth0410-248

Afzal, A. R., Rajab, A., Fenske, C. D., Oldridge, M., Elanko, N., Ternes-Pereira, E., Tüysüz, B., Murday, V. A., Patton, M. A., Wilkie, A. O., & Jeffery, S. (2000). Recessive Robinow syndrome, allelic to dominant

brachydactyly type B, is caused by mutation of *ROR2*. *Nature Genetics*, *25*(4), 419–422. https://doi.org/10.1038/78107

Aglan, M., Amr, K., Ismail, S., Ashour, A., Otaify, G. A., Mehrez, M. A., Aboul-Ezz, E. H., El-Ruby, M., Mazen, I., Abdel-Hamid, M. S., & Temtamy, S. A. (2015). Clinical and molecular characterization of seven Egyptian families with autosomal recessive Robinow syndrome: Identification of four novel *ROR2* gene mutations. *American Journal of Medical Genetics Part A*, *167A*(12), 3054–3061. https://doi.org/10.1002/ajmg.a.37287

Ali, B. R., Jeffery, S., Patel, N., Tinworth, L. E., Meguid, N., Patton, M. A., & Afzal, A. R. (2007). Novel Robinow syndrome causing mutations in the proximal region of the frizzled-like domain of *ROR2* are retained in the endoplasmic reticulum. *Human Genetics*, *122*(3-4), 389–395. https://doi.org/10.1007/s00439-007-0409-0

Beck, C. R., Carvalho, C., Akdemir, Z. C., Sedlazeck, F. J., Song, X., Meng, Q., Hu, J., Doddapaneni, H., Chong, Z., Chen, E. S., Thornton, P. C., Liu, P., Yuan, B., Withers, M., Jhangiani, S. N., Kalra, D., Walker, K., English, A. C., … Lupski, J. R. (2019). Megabase length hypermutation accompanies human structural variation at 17p11.2. *Cell*, *176*(6), 1310–1324. https://doi.org/10.1016/j.cell.2019.01.045

Beiraghi, S., Leon-Salazar, V., Larson, B. E., John, M. T., Cunningham, M. L., Petryk, A., & Lohr, J. L. (2011). Craniofacial and intraoral phenotype of Robinow syndrome forms. *Clinical Genetics*, *80*(1), 15–24. https://doi.org/10.1111/j.1399-0004.2011.01683.x

Ben-Shachar, S., Khajavi, M., Withers, M. A., Shaw, C. A., van Bokhoven, H., Brunner, H. G., & Lupski, J. R. (2009). Dominant versus recessive traits conveyed by allelic mutations–to what extent is nonsense-mediated decay involved? *Clinical Genetics*, *75*(4), 394–400. https://doi.org/10.1111/j.1399-0004.2008.01114.x

Birgmeier, J., Esplin, E. D., Jagadeesh, K. A., Guturu, H., Wenger, A. M., Chaib, H., Buckingham, J. A., Bejerano, G., & Bernstein, J. A. (2018). Biallelic loss-of-function *WNT5A* mutations in an infant with severe and atypical manifestations of Robinow syndrome. *American Journal of Medical Genetics, Part A*, *176*(4), 1030–1036. https://doi.org/10.1002/ajmg.a.38636

Bunn, K. J., Daniel, P., Rösken, H. S., O'Neill, A. C., Cameron-Christie, S. R., Morgan, T., Brunner, H. G., Lai, A., Kunst, H. P., Markie, D. M., & Robertson, S. P. (2015). Mutations in *DVL1* cause an osteosclerotic form of Robinow syndrome. *American Journal of Human Genetics*, *96*(4), 623–630. https://doi.org/10.1016/j.ajhg.2015.02.010

Carvalho, C. M., & Lupski, J. R. (2016). Mechanisms underlying structural variant formation in genomic disorders. *Nature Reviews Genetics*, *17*(4), 224–238. https://doi.org/10.1038/nrg.2015.25

Chen, Y., Bellamy, W. P., Seabra, M. C., Field, M. C., & Ali, B. R. (2005). ER-associated protein degradation is a common mechanism underpinning numerous monogenic diseases including Robinow syndrome. *Human Molecular Genetics*, *14*(17), 2559–2569. https://doi.org/10.1093/hmg/ddi259

Conlon, C. J., Abu-Ghname, A., Raghuram, A. C., Davis, M. J., Guillen, D. E., Sutton, V. R., Carvalho, C., & Maricevich, R. S. (2021). Craniofacial phenotypes associated with Robinow syndrome. *American Journal of Medical Genetics, Part A*, *185*(12), 3606–3612. https://doi.org/10.1002/ajmg.a.61986

Eldomery, M. K., Coban-Akdemir, Z., Harel, T., Rosenfeld, J. A., Gambin, T., Stray-Pedersen, A., Küry, S., Mercier, S., Lessel, D., Denecke, J., Wiszniewski, W., Penney, S., Liu, P., Bi, W., Lalani, S. R., Schaaf, C. P., Wangler, M. F., Bacino, C. A., Lewis, R. A., … Lupski, J. R. (2017). Lessons learned from additional research analyses of unsolved clinical exome cases. *Genome Medicine*, *9*(1), 26. https://doi.org/10.1186/s13073-017-0412-6

Geetha-Loganathan, P., Nimmagadda, S., Antoni, L., Fu, K., Whiting, C. J., Francis-West, P., & Richman, J. M. (2009). Expression of WNT signalling pathway genes during chicken craniofacial development. *Developmental Dynamics*, *238*(5), 1150–1165. https://doi.org/10.1002/dvdy.21934

Gerber, J. A., Sheth, K. R., & Austin, P. F. (2021). Robinow syndrome: Genital analysis, genetic heterogeneity, and associated psychological impact. *American Journal of Medical Genetics, Part A*, *185*(12), 3601–3605. https://doi.org/10.1002/ajmg.a.61981

Kircher, M., Witten, D. M., Jain, P., O'Roak, B. J., Cooper, G. M., & Shendure, J. (2014). A general framework for estimating the relative pathogenicity of human genetic variants. *Nature Genetics*, *46*(3), 310–315. https://doi.org/10.1038/ng.2892

Lin, D. (1998). An information-theoretic definition of similarity. *International Conference on Malignant Lymphom*, *98*, 296-304. https://doi.org/10.5555/645527.657297

Liu, P., Meng, L., Normand, E. A., Xia, F., Song, X., Ghazi, A., Rosenfeld, J., Magoulas, P. L., Braxton, A., Ward, P., Dai, H., Yuan, B., Bi, W., Xiao, R., Wang, X., Chiang, T., Vetrini, F., He, W., Cheng, H., … Yang, Y. (2019). Reanalysis of clinical exome sequencing data. *The New England Journal of Medicine*, *380*(25), 2478–2480. https://doi.org/10.1056/NEJMc1812033

Lupski, J. R. (2021). Clan genomics: From OMIM phenotypic traits to genes and biology. *American Journal of Medical Genetics, Part A*, *185*(11), 3294–3313. https://doi.org/10.1002/ajmg.a.62434

Lupski, J. R., Belmont, J. W., Boerwinkle, E., & Gibbs, R. A. (2011). Clan genomics and the complex architecture of human disease. *Cell*, *147*(1), 32–43. https://doi.org/10.1016/j.cell.2011.09.008

Mazzeu, J. F., Pardono, E., Vianna-Morgante, A. M., Richieri-Costa, A., Ae Kim, C., Brunoni, D., Martelli, L., de Andrade, C. E., Colin, G., & Otto, P. A. (2007). Clinical characterization of autosomal dominant and recessive variants of Robinow syndrome. *American Journal of Medical Genetics, Part A*, *143*(4), 320–325. https://doi.org/10.1002/ajmg.a.31592

Mehawej, C., Chouery, E., Maalouf, D., Baujat, G., Le Merrer, M., Cormier-Daire, V., & Mégarbané, A. (2012). Identification of a novel causative mutation in the *ROR2* gene in a Lebanese family with a mild form of recessive Robinow syndrome. *European Journal of Medical Genetics*, *55*(2), 103–108. https://doi.org/10.1016/j.ejmg.2011.11.003

Nohno, T., Kawakami, Y., Wada, N., Komaguchi, C., & Nishimatsu, S. (1999). Differential expression of the frizzled family involved in Wnt signaling during chick limb development. *Cellular and Molecular Biology*, *45*(5), 653–659.

Person, A. D., Beiraghi, S., Sieben, C. M., Hermanson, S., Neumann, A. N., Robu, M. E., Schleiffarth, J. R., Billington, C. J., Jr., van Bokhoven, H., Hoogeboom, J. M., Mazzeu, J. F., Petryk, A., Schimmenti, L. A., Brunner, H. G., Ekker, S. C., & Lohr, J. L. (2010). *WNT5A* mutations in patients with autosomal dominant Robinow syndrome. *Developmental Dynamics*, *239*(1), 327–337. https://doi.org/10.1002/dvdy.22156

Posey, J. E., O'Donnell-Luria, A. H., Chong, J. X., Harel, T., Jhangiani, S. N., Coban Akdemir, Z. H., Buyske, S., Pehlivan, D., Carvalho, C., Baxter, S., Sobreira, N., Liu, P., Wu, N., Rosenfeld, J. A., Kumar, S., Avramopoulos, D., White, J. J., Doheny, K. F., Witmer, P. D., … Centers for Mendelian. (2019). Insights into genetics, human biology and disease gleaned from family based genomic studies. *Genetics in Medicine: Official Journal of the American College of Medical Genetics*, *21*(4), 798–812. https://doi.org/10.1038/s41436-018-0408-7

Reid, J. G., Carroll, A., Veeraraghavan, N., Dahdouli, M., Sundquist, A., English, A., Bainbridge, M., White, S., Salerno, W., Buhay, C., Yu, F., Muzny, D., Daly, R., Duyk, G., Gibbs, R. A., & Boerwinkle, E. (2014). Launching genomics into the cloud: Deployment of Mercury, a next generation sequence analysis pipeline. *BMC Bioinformatics*, *15*, 30. https://doi.org/10.1186/1471-2105-15-30

Richards, S., Aziz, N., Bale, S., Bick, D., Das, S., Gastier-Foster, J., Grody, W. W., Hegde, M., Lyon, E., Spector, E., Voelkerding, K., Rehm, H. L., & ACMG Laboratory Quality Assurance Committee. (2015). Standards and guidelines for the interpretation of sequence variants: A joint consensus recommendation of the American

College of Medical Genetics and Genomics and the Association for Molecular Pathology. *Genetics in Medicine*, *17*(5), 405–424. https://doi.org/10.1038/gim.2015.30

Robinow, M., Silverman, F. N., & Smith, H. D. (1969). A newly recognized dwarfing syndrome. *American Journal of Diseases of Children*, *117*(6), 645–651. https://doi.org/10.1001/archpedi.1969.02100030647005

Sassa, A., Kanemaru, Y., Kamoshita, N., Honma, M., & Yasui, M. (2016). Mutagenic consequences of cytosine alterations site-specifically embedded in the human genome. *Genes and Environment*, *38*(1), 17. https://doi.org/10.1186/s41021-016-0045-9

Schwabe, G. C., Tinschert, S., Buschow, C., Meinecke, P., Wolff, G., Gillessen-Kaesbach, G., Oldridge, M., Wilkie, A. O., Kömec, R., & Mundlos, S. (2000). Distinct mutations in the receptor tyrosine kinase gene *ROR2* cause brachydactyly type B. *American Journal of Human Genetics*, *67*(4), 822–831. https://doi.org/10.1086/303084

Schwabe, G. C., Trepczik, B., Süring, K., Brieske, N., Tucker, A. S., Sharpe, P. T., Minami, Y., & Mundlos, S. (2004). *Ror2* knockout mouse as a model for the developmental pathology of autosomal recessive Robinow syndrome. *Developmental Dynamics*, *229*(2), 400–410. https://doi.org/10.1002/dvdy.10466

Schwartz, D. D., Fein, R. H., Carvalho, C., Sutton, V. R., Mazzeu, J. F., & Axelrad, M. E. (2021). Neurocognitive, adaptive, and psychosocial functioning in individuals with Robinow syndrome. *American Journal of Medical Genetics, Part A*, *185*(12), 3576–3583. https://doi.org/10.1002/ajmg.a.61854

Shayota, B. J., Zhang, C., Shypailo, R. J., Mazzeu, J. F., Carvalho, C., & Sutton, V. R. (2020). Characterization of the Robinow syndrome skeletal phenotype, bone micro-architecture, and genotype-phenotype correlations with the osteosclerotic form. *American Journal of Medical Genetics, Part A*, *182*(11), 2632–2640. https://doi.org/10.1002/ajmg.a.61843

Sim, N. L., Kumar, P., Hu, J., Henikoff, S., Schneider, G., & Ng, P. C. (2012). SIFT web server: Predicting effects of amino acid substitutions on proteins. *Nucleic Acids Research*, *40*, W452–W457. https://doi.org/10.1093/nar/gks539

Sisson, B. E., & Topczewski, J. (2009). Expression of five frizzleds during zebrafish craniofacial development. *Gene Expression Patterns*, *9*(7), 520–527. https://doi.org/10.1016/j.gep.2009.07.003

Song, X., Beck, C. R., Du, R., Campbell, I. M., Coban-Akdemir, Z., Gu, S., Breman, A. M., Stankiewicz, P., Ira, G., Shaw, C. A., & Lupski, J. R. (2018). Predicting human genes susceptible to genomic instability associated with Alu/Alu-mediated rearrangements. *Genome Research*, *28*(8), 1228–1242. https://doi.org/10.1101/gr.229401.117

Stricker, S., Rauschenberger, V., & Schambony, A. (2017). ROR-family receptor tyrosine kinases. *Current Topics in Developmental Biology*, *123*, 105–142. https://doi.org/10.1016/bs.ctdb.2016.09.003

van Bokhoven, H., Celli, J., Kayserili, H., van Beusekom, E., Balci, S., Brussel, W., Skovby, F., Kerr, B., Percin, E. F., Akarsu, N., & Brunner, H. G. (2000). Mutation of the gene encoding the ROR2 tyrosine kinase causes autosomal recessive Robinow syndrome. *Nature Genetics*, *25*(4), 423–426. https://doi.org/10.1038/78113

Wadia, R. S., Shirole, D. B., & Dikshit, M. S. (1978). Recessively inherited costovertebral segmentation defect with mesomelia and peculiar facies (Covesdem syndrome): A new genetic entity? *Journal of Medical Genetics*, *15*(2), 123–127. https://doi.org/10.1136/jmg.15.2.123

Ward, J. H. (1963). Hierarchical grouping to optimize an objective function. *Journal of the American Statistical Association*, *58*, 236–244.

White, J. J., Mazzeu, J. F., Coban-Akdemir, Z., Bayram, Y., Bahrambeigi, V., Hoischen, A., van Bon, B. W. M., Gezdirici, A., Gulec, E. Y., Ramond, F., Touraine, R., Thevenon, J., Shinawi, M., Beaver, E., Heeley, J., Hoover-Fong, J., Durmaz, C. D., Karabulut, H. G., Marzioglu-Ozdemir, E., … Carvalho, C. M. B. (2018). WNT signaling perturbations underlie the genetic heterogeneity of Robinow Syndrome. *American Journal of Human Genetics*, *102*(1), 27–43. https://doi.org/10.1016/j.ajhg.2017.10.002

White, J. J., Mazzeu, J. F., Hoischen, A., Bayram, Y., Withers, M., Gezdirici, A., Kimonis, V., Steehouwer, M., Jhangiani, S. N., Muzny, D. M., Gibbs, R. A., Baylor-Hopkins Center, Mendelian Genomicsvan Bon, B., Sutton, V. R., Lupski, J. R., Brunner, H. G., & Carvalho, C. (2016). *DVL3* alleles resulting in a -1 frameshift of the last exon mediate autosomal-dominant Robinow syndrome. *American Journal of Human Genetics*, *98*(3), 553–561. https://doi.org/10.1016/j.ajhg.2016.01.005

White, J. J., Mazzeu, J. F., Hoischen, A., Jhangiani, S. N., Gambin, T., Alcino, M. C., Penney, S., Saraiva, J. M., Hove, H., Skovby, F., Kayserili, H., Estrella, E., Vulto-van Silfhout, A. T., Steehouwer, M., Muzny, D. M., Sutton, V. R., Gibbs, R. A., Baylor-Hopkins Center for Mendelian, G., Lupski, J. R., … Carvalho, C. M. (2015). *DVL1* frameshift mutations clustering in the penultimate exon cause autosomal-dominant Robinow syndrome. *American Journal of Human Genetics*, *96*(4), 612–622. https://doi.org/10.1016/j.ajhg.2015.02.015

Zhang, C., Jolly, A., Shayota, B. J., Mazzeu, J. F., Du, H., Dawood, M., Soper, P. C., Ramalho de Lima, A., Ferreira, B. M., Coban-Akdemir, Z., White, J., Shears, D., Thomson, F. R., Douglas, S. L., Wainwright, A., Bailey, K., Wordsworth, P., Oldridge, M., Lester, T., … Carvalho, C. (2022). Novel pathogenic variants and quantitative phenotypic analyses of Robinow syndrome: WNT signaling perturbation and phenotypic variability. *HGG Advances*, *3*(1):100074. https://doi.org/10.1016/j.xhgg.2021.100074

Zhang, C., Mazzeu, J. F., Eisfeldt, J., Grochowski, C. M., White, J., Akdemir, Z. C., Jhangiani, S. N., Muzny, D. M., Gibbs, R. A., Lindstrand, A., Lupski, J. R., Sutton, V. R., & Carvalho, C. (2021). Novel pathogenic genomic variants leading to autosomal dominant and recessive Robinow syndrome. *American Journal of Medical Genetics, Part A*, *185*(12), 3593–3600. https://doi.org/10.1002/ajmg.a.61908

SUPPORTING INFORMATION

Additional supporting information can be found online in the Supporting Information section at the end of this article.

How to cite this article: Lima, A. R., Ferreira, B. M., Zhang, C., Jolly, A., Du, H., White, J. J., Dawood, M., Lins, T. C., Chiabai, M. A., van Beusekom, E., Cordoba, M. S., Caldas Rosa, E. C. C., Kayserili, H., Kimonis, V., Wu, E., Mellado, C., Aggarwal, V., Richieri-Costa, A., Brunoni, D., … Mazzeu, J. F. (2022). Phenotypic and mutational spectrum of *ROR2*-related Robinow syndrome. *Human Mutation*, 1–19. https://doi.org/10.1002/humu.24375